ISSN 1063-7761, Journal of Experimental and Theoretical Physics, 2008, Vol. 107, No. 2, pp. 251–262. © Pleiades Publishing, Inc., 2008.
Original Russian Text © V.S. Edelman, 2008, published in Zhurnal Éksperimental'noĭ i Teoreticheskoĭ Fiziki, 2008, Vol. 134, No. 2, pp. 298–309.

ELECTRONIC PROPERTIES OF SOLIDS

Tunneling Spectra at Terrace Boundaries on the Bismuth Surface

V. S. Edelman

Kapitza Institute for Physical Problems, Russian Academy of Sciences, ul. Kosygina 2, Moscow, 119334 Russia
e-mail: edelman@kapitza.ras.ru

Received December 25, 2007

Abstract—The scanning tunneling spectra of the trigonal bismuth surface are measured in the vicinity of the boundaries of terraces with a diatomic height. It is found that the tunneling spectrum of the planar surface begins to transform at a distance of 2–3 nm from the terrace boundaries, specific features that are characteristic of the planar surface far from the terrace boundaries disappear, and new peaks in the density of states are observed. An analysis of the behavior of the current–voltage characteristics has revealed that one-dimensional electronic systems with a width of the order of an interatomic distance with their own individual spectra are formed at the ends of the rows of the atomic planes.

PACS numbers: 73.20.At, 73.20.-r

DOI: 10.1134/S1063776108080098

1. INTRODUCTION

The electronic properties of bismuth have been investigated over many decades. The energy spectrum of conduction electrons in the bulk of this material has been studied in sufficient detail (see the review [1]). Significant advances have been made in calculating the band structure [2]. The results of these calculations in the most sensitive region, i.e., in the vicinity of the Fermi surface, are in remarkable agreement with experimental data, which requires the accuracy in calculating the energy at the level of a millielectronvolt. Considerable progress has been achieved in the study of surface states. In particular, the investigation of two atomic faces, namely, the trigonal (111) surface (perpendicular to the Γ–T direction in the traditional notation [2]) and the "pseudotrigonal" twin surface (perpendicular to one of the three equivalent Γ–L directions), which coexist with the trigonal surface on a cleavage of the bismuth crystal, was performed using scanning tunneling spectroscopy in [3]. It was shown that, at the surface, there exist two-dimensional electronic states with the characteristics dependent on the surface orientation. In a number of works (see [4–7] and references therein), three bismuth faces, (111), (110), and (100), were examined by angle-resolved photoelectron spectroscopy. In those studies, reliable data were obtained on the density of two-dimensional states near the Fermi level and their spectra were calculated theoretically.

According to the results of the aforementioned works, the two-dimensional character of surface states with a density considerably higher than the anomalously low density of conduction electrons in the bulk of bismuth can be considered to be reliably established experimentally [1]. The formation of these states is associated with the violation of the translational symmetry of the crystal because of the presence of a free surface. This inference is confirmed by the calculations performed in [5–7], which somewhat differ in both the initial assumptions (in particular, those regarding the degree of the influence of the spin–orbit interaction) and numerical results.

One of the obvious directions of further research in the field under consideration consists in investigating electronic characteristics of surface defects. Some defects, for example, defects located below the surface, can be revealed only from variations in tunneling spectra [8], whereas other defects, such as extended terraces with a diatomic height, nanoislands, hollows, macroscopic and microscopic twin interlayers, and dislocation outcrops, can be found using scanning tunneling microscopy [9]. It is clear that two-dimensional surface states should be transformed as the boundaries of atomically smooth terraces are approached at a distance of the order of $\pi/k \approx 1$–3 nm (where k is the wave vector of two-dimensional electrons, which at the Fermi level is on the order of 1–3 nm^{-1} [5, 7]). At the boundaries themselves, there can arise one-dimensional electronic states [9–11]. This paper is devoted to the study of these states by scanning tunneling spectroscopy.

Scanning tunneling spectroscopy, i.e., measurement of local current–voltage characteristics with the use of a scanning tunneling microscope (STM), makes it possible to examine the surface under investigation in sufficient detail and to draw reliable conclusions regarding the structure and properties of this surface, especially in the case of samples prepared under the conditions of deep vacuum. Moreover, the method has the advantage that scanning tunneling spectroscopy provides a means for studying the electronic spectrum with a high spatial (up to atomic) resolution. Of course, this method is combined with scanning tunneling microscopy, which

permits one to compare the obtained results with the actual structure of the surface. In this case, it is desirable to perform investigations at low temperatures in order to avoid thermal smearing of spectral features at low energies and to decrease the probability of tunneling with emission of phonons. This approach, as applied to bismuth, enables one to avoid problems associated with thermal motion of boundaries of atomic terraces [9]. It is particularly important that, when samples are prepared by in situ cleaving of crystals at low temperatures, there can arise terraces with straight almost atomically smooth boundaries, macroscopic twins, and twin interlayers with quantized width and ideal boundaries [8–10]. These objects are physically well defined, which opens up new possibilities for detailed investigations.

2. SAMPLES PREPARATION AND EXPERIMENTAL TECHNIQUE

For our investigations, samples were prepared in the form of long rods oriented along the trigonal axis. Samples approximately $1 \times 2 \times 5$ mm^3 in size were cut on an electric-spark machine from single crystals grown from a melt of the initial material with a purity of 99.99999% according to the procedure described in [12]. For this purity, the concentration of impurity atoms on the cleavage surface should lie in the range 1–10 atoms/μm^2. The dislocation density determined on the crystal cleavage from etch pits by etching in a dilute nitric acid was on the order of 0.05 μm^{-2}. When cutting the sample, a shallow incision was made at its half-height with the aim of specifying the position of the cleavage surface. The samples were etched in nitric acid in order to remove the contaminated surface layer and then were washed in distilled water.

The investigations were performed on a low-temperature setup [13] with the use of a scanning tunneling microscope [14]. In contrast to the design of the microscope described in [14], piezoelectric inertial step motors were replaced by a single three-coordinate displacement system based on the effect of electrodynamic forces [15]. The specific feature of the scanning tunneling microscope is the possibility of displacing a tip along three directions in steps from several fractions of a millimeter to several millimeters under the control of a computer. Therefore, the surface region under investigation can be chosen with a size within the range of typical sample sizes of the order of 1–2 mm by means of the observation of the sample under the microscope through optical windows of the cryostat. By this means, it is possible to examine several tens of regions, i.e., in actual fact, several tens of different samples, in one cryogenic experiment. The sample mounted in the scanning tunneling microscope could be in situ broken at low temperatures under the conditions of deep vacuum or in a heat-exchange gas (helium) medium. The measurements were carried out at the temperature of the sample in the vicinity of the helium boiling point.

An STM tip was cut from a wire (Pt + 6% Rh) by scissors. As a rule, this resulted in the formation of multipoint tips, which, however, made it possible to achieve the true tunneling contact. Unfortunately, the tips prepared by electrochemical etching with subsequent ion sputtering did not ensure a tunneling contact at low temperatures. The electric current appeared only in the case of mechanical contact. This phenomenon can be explained by freeze-out of conduction of the damaged surface layer of the tip.

The STM images and current–voltage characteristics were obtained by the traditional method under the control of a computer with the use of an *L*-card ADC–DAC board (Moscow, Russia) providing the digital feedback. In order to increase the signal-to-noise ratio, each current–voltage characteristic was recorded many times and the results thus obtained were averaged. As a rule, the number of measurements was equal to 50–100 and the time required to measure one current–voltage characteristic was approximately 5 s. The measured currents were on the order of 0.3–0.6 nA, and the noises of the order of 1–2% were predominantly caused by mechanical vibrations.

In the first experiments, after the STM images were obtained and specific features of the surface relief (such as terrace boundaries) were revealed, a set of current–voltage characteristics was measured at points with the coordinates specified by the operator. This procedure took much time; as a result, with allowance made for the drift of the scanning tunneling microscope, the correspondence of the results to the specific features of the surface relief was not very reliable. Subsequently, we developed a procedure for measuring a set of current–voltage characteristics along a line on the surface of the sample with specified values of the tip displacement step and the step number.

For the most part, the measurements were performed under the conditions where the voltage $U_{\mathrm{Bi}\text{–}tip}$ between the bismuth sample and the tip was varied from +0.65 to –0.65 V. A number of measurements were carried out at voltages ranging from +1.8 to –1.8 V. At each step of the displacement of the STM tip along the x coordinate, when the feedback controlling the position of the tip along the z coordinate perpendicular to the surface was "switched on" and the voltage in the chosen range was maximum, the tunneling gap was established so that the electric current was equal to a specified value. Then, the z coordinate was written, the STM feedback was "switched off" (and, hence, the value of z was fixed), and the tunneling current I was measured at the voltage $U_{\mathrm{Bi}\text{–}tip}$ decreasing in specified steps. After the minimum voltage was reached, the voltage was restored to its initial value, the feedback was switched on, and the procedure was repeated a specified

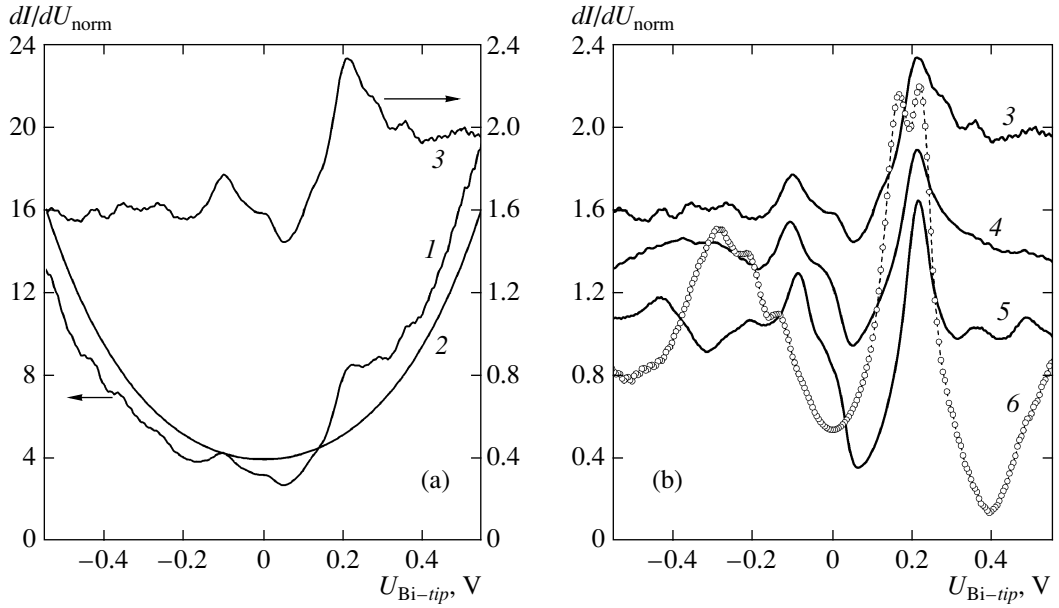

Fig. 1. Differential current–voltage characteristics obtained for planar surface regions in different experiments: (*1*) derivative of the experimental current–voltage characteristic, (*2*) derivative of the fitting function $I_0 \sinh(U_{\text{Bi}-tip}/W)$, (*3–5*) normalized differential current–voltage characteristics for the trigonal plane, and (*6*) differential current–voltage characteristic for the quasi-trigonal plane (the surface of the twin interlayer). Conditions: (*1*, *3*) $I \approx 6$ nA at the voltage $U_{\text{Bi}-tip} = -0.6$ V and the parameter $W = 0.26$ V; (*4*) $I = 1.8$ nA, $W = 0.34$ V; (*5*) $I = 0.3$ nA, $W = 0.56$ V; and (*6*) $I = 0.5$ nA, $W = 0.56$ V. Current–voltage characteristics *3* and *4* are shifted along the *y* axis by 0.8 and 0.4, respectively.

number of times. Thereafter, the result averaged over all measurements, i.e., the dependence $I(U_{\text{Bi}-tip})$, was written in the computer memory and the tip was displaced by the next step along the *x* coordinate. After the completion of each cycle, the corresponding two-dimensional data array was formed so that the first row contained data on the dependence $z(x)$ and the first column involved voltages at which the currents were measured. The other rows included data on the dependence of the current on the coordinate at the relevant voltage, and the columns of the matrix contained data on the current–voltage characteristics at the corresponding *x* coordinate.

The results of measurements were processed with the ORIGIN program package, which made it possible to perform the differentiation of the current–voltage characteristics with smoothing, their summation, averaging, and other operations. The resolution of the specific features in the current–voltage characteristics was determined by the number of points in these curves (usually, 127 or 255) and the smoothing parameter, which was chosen from the compromise between a sufficiently strong suppression of high-frequency noise and a small broadening of narrow lines.

3. RESULTS

In scanning tunneling spectroscopy, it is very important to separate the effects associated with the sample itself from the effects caused by the properties of the scanning tip. This problem is not very simple because nothing is actually known about the tip. Indeed, neither the shape nor even the material of the tip end on the atomic scale can be determined experimentally. For example, the tip can end not with platinum (or rhodium) atoms but with any atoms sorbed on the tip surface or with a sample particle trapped upon accidental contact with the surface. Therefore, the only solution of the problem is to compare the results obtained from different experiments. When the experimental conditions (such as the electric current) in this situation are likewise different, it is possible to evaluate the effect coming from the interaction with the tip on the spectra (it is obvious that this effect correlates with the current strength).

In our investigations, we performed several tens of experiments. As a rule, we used in this case multipoint tips. The current–voltage characteristics measured with different tips and the calculated differential current–voltage characteristics differ in shape, and, as can be seen from Fig. 1a (curve *1*), the exponential contribution to the current–voltage characteristic with increasing voltage becomes dominant. This contribution comes from the increase in the transparency of the tunnel barrier [3, 16], because, to a first approximation, the transparency of the tunnel barrier increases as $\exp(U_{\text{Bi}-tip}/W)$, where *W* is the parameter characterizing the work function of the tip and the sample. In order to

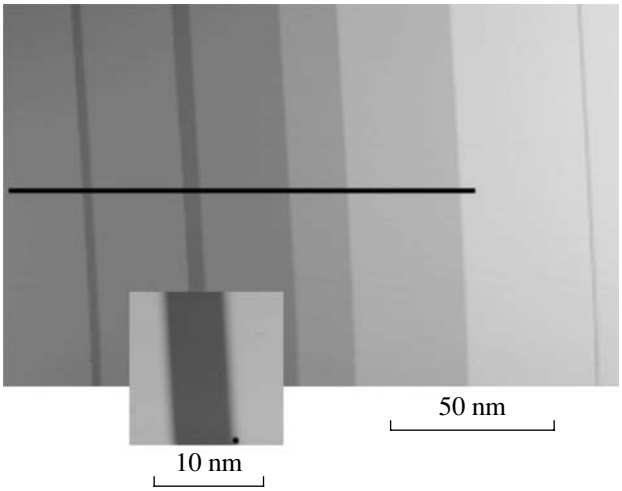

Fig. 2. STM image of a bismuth surface region studied by scanning tunneling spectroscopy in the vicinity of the terrace boundaries. The current–voltage characteristics were measured with the displacement of the STM tip along the black line in the topogram. The dot in the frame recorded with a larger magnification corresponds to the size of the region per atom. The absence of fractures in the terrace boundary on this scale indicates an atomic smoothness of the boundary. The total change in the contrast from bright to dark in the large frame corresponds to 2 nm.

eliminate this exponential contribution, the experimental current–voltage characteristic averaged over many measurements was approximated by the fitting relationship

$$I_{\text{fit}} = I_0 \sinh(U_{\text{Bi}-tip}/W),$$

and the derivative of the current–voltage characteristic with respect to the voltage was smoothed over several points and normalized to the same derivative of the current I_{fit} (Fig. 1a, curve *2*). This procedure leads to approximately the same results as those obtained within the approach proposed by Stroscio and Feenstra [16] for the calculation of the logarithmic derivative of the current with respect to the voltage. However, the former approach is more convenient because it leads to a decrease in the contribution from the change in the barrier transparency and, at the same time, does not lead to an uncertainty in the vicinity of zero voltage, i.e., in the most interesting range. Owing to the normalization, we obtain the dimensionless differential current–voltage characteristic dI/dU_{norm} (Fig. 1a, curve *3*). This allows a quantitative comparison of the results obtained from different experiments under different initial conditions of the measurement of the current–voltage characteristics.

The correctness of the normalization procedure is confirmed by comparing the differential current–voltage characteristics measured in different experiments (Fig. 1b). It should be noted that the parameters W for the three presented characteristics differ significantly. In the case under consideration, the normalization of characteristic *5* in Fig. 1 leaves its shape almost unchanged, especially in the voltage range from –0.3 to 0.2 V, where all three characteristics obtained for the trigonal surface are very similar to each other. According to [16], the broadening of the peaks in these characteristics with an increase in the current (and, hence, a decrease in the distance between the tip and the sample) is quite expectable. The differences between the characteristics at higher voltages are associated either with the noise (the noise contribution increases proportionally with the current) or with the specific features of the matrix elements of the overlap of the wave functions, provided their symmetry is different for different tips.

Therefore, the structure of normalized differential current–voltage characteristics *3–5* near the Fermi level does not depend on the tip and is determined only by the bismuth surface. This conclusion is additionally supported by a comparison with differential current–voltage characteristic *6* (obtained in [3]) for the surface of the twin interlayer that has a different orientation. This differential current–voltage characteristic in the vicinity of the Fermi level exhibits a substantially different behavior.

Now, we turn to the discussion of the results obtained in the vicinity of the terrace boundaries. For the most part, these results were obtained in the course of one series of measurements performed for several hours on the same surface region of the surface. The topogram of this surface region is displayed in Fig. 2. The choice of this set of data for the analysis was motivated by the following circumstances:

(1) The presence of several terraces with straight boundaries on the atomic scale makes it possible to carry out measurements for different boundaries and to compare the results obtained. The smoothness of the boundaries suggests that they have a one-dimensional character.

(2) In contrast to other experiments, this series of measurements was carried out, fortunately, with the use of a single-point tip, as could be judged from both the equality of the height differences upon intersection of all visible boundaries and the absence of double boundaries that are characteristic of multipoint tips.

(3) The effect of a change in the barrier transparency with an increase in the voltage was weaker than that in other experiments, the changes introduced into differential current–voltage characteristics by the normalization at voltages from –0.5 to 0.5 V left their shape almost unchanged, and the highest resolution of the specific features was achieved.

(4) By the time of the performance of these experiments, we developed the aforementioned procedure specially for simultaneously measuring the current–voltage characteristics and the dependence $z(x)$, which eliminated an uncertainty in the correspondence of the results to the surface relief.

Sets of current–voltage characteristics were measured with the displacement of the STM tip (Pt + 6%

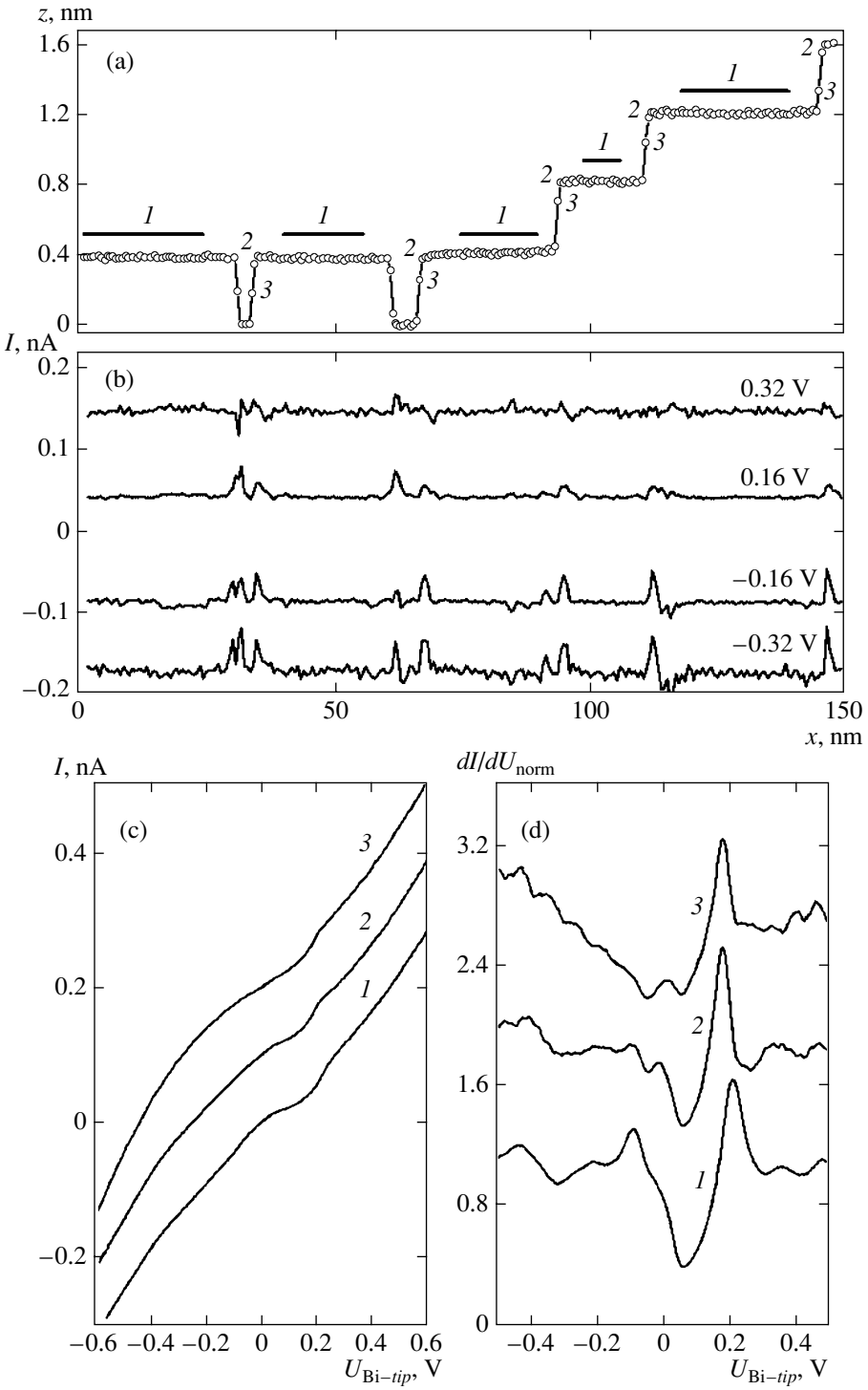

Fig. 3. (a) Dependence $z(x)$ of the displacement of the STM tip along the vertical axis and (b) dependences of the current $I(x)$ at several voltages across the tunneling gap on the coordinate along the black line marked in Fig. 2, (c) current–voltage characteristics, and (d) differential current–voltage characteristics averaged for the points denoted by the corresponding numerals in the dependence $z(x)$.

Rh) along the black line shown in the topogram displayed in Fig. 2. This line intersects several atomically straight boundaries of the terraces. It is worth noting that there are both descending and ascending regions along the scanning path (Fig. 3a). In the dependences $I(x)$ at fixed voltages, specific features appear every time when the tip intersects the terrace boundaries (Fig. 3b). These specific features are not related to the change in the tunneling conditions with a change in the surface curvature. If the probability of tunneling in this

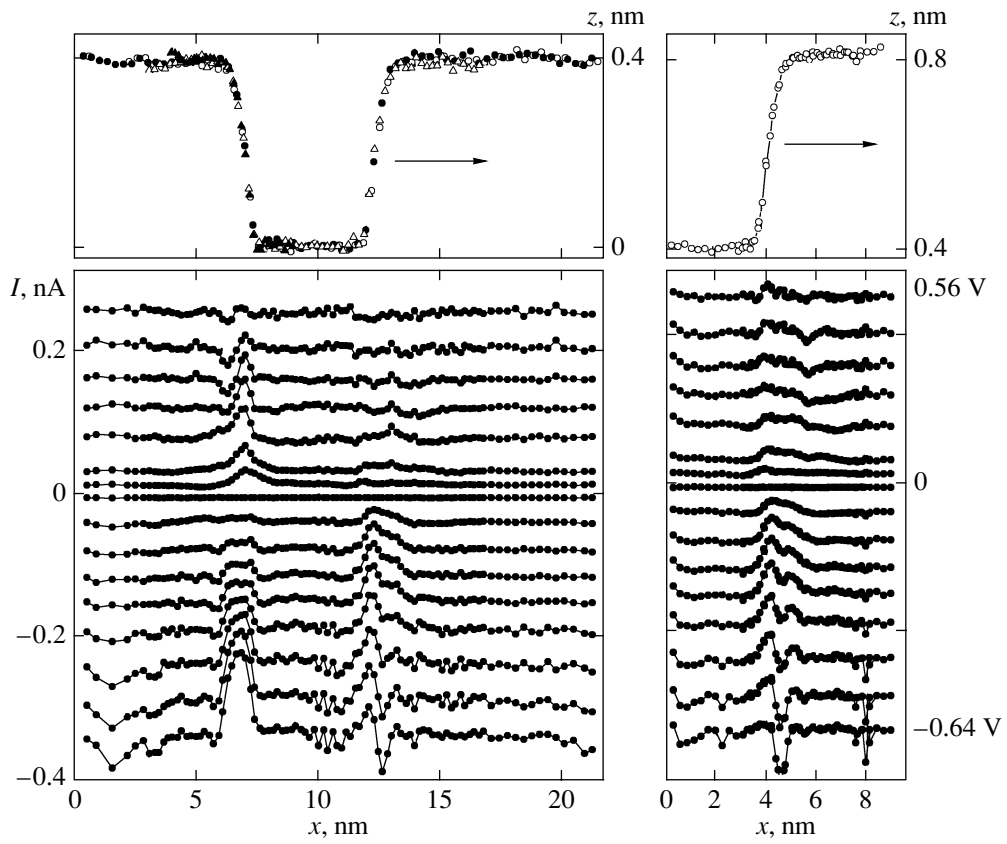

Fig. 4. Dependences $z(x)$ and $I(x)$ for the valley (in the region close to 60 nm in Fig. 3a) (at the left) and dependences $z(x)$ and $I(x)$ for the step (in the vicinity of 90 nm in Fig. 3a) (at the right). Different symbols in the upper left panel correspond to the data obtained in different cycles of measurements with different steps along the x axis (four cycles for the descending region and three cycles for the ascending region). The values of the current are averaged over these cycles. The lower left panel presents the results averaged over two cycles.

case changes, the change is automatically taken into account by the procedure used for measuring the current–voltage characteristic, because it specifies the initial value of the current at a specified voltage. As can be seen from Fig. 3c and especially clearly from Fig. 3d, the variation in the current–voltage characteristic, i.e., the variation in the spectrum of electronic states, is responsible for the change in the current.

The current–voltage characteristics shown in Fig. 3 correspond to three typical regions: planar regions far from the terrace boundaries, the upper edge of the terraces, and approximately the midpoint of the step. In each of these three regions, the current–voltage characteristics coincide accurate to within noises. This circumstance permits us to average the current–voltage characteristics with the aim of decreasing the noise level. It can be seen from Fig. 3 that, upon changing over from the plane to the step, the peak located at 0.21 V above the Fermi level gives way to the peak in the range 0.18–0.19 V, the inflection at zero transforms into a maximum, and the peak at –0.1 V disappears.

Small portions of the path in the vicinity of the wider "valley" (Fig. 3a, $x \approx$60–65 nm) and the nearest step to the right of it ($x \approx 90$ nm) were scanned several times with a higher spatial resolution as compared to that in Fig. 3. This made it possible to thoroughly trace the evolution of the tunneling spectra in narrow regions (with a width of approximately only 1 nm) characterized by an abrupt change in the surface relief. Figure 4 shows the dependences $z(x)$ and $I(x)$ for these regions. These dependences were constructed with allowance made for the small drift (less than 0.5 nm along the x coordinate and less than 0.1 nm along the z coordinate) observed in sequential scans: we introduced the correction for these coordinates that provided the coincidence of the dependences $z(x)$.

It can be seen that the current characteristics for the "descending" and "ascending" regions differ significantly. For example, at negative voltages, there is a well-defined maximum with a width of approximately 1.5 nm in the descending region and a small maximum in the ascending region gives way to a minimum with a width smaller than 1 nm. At positive voltages, the differences are also noticeable. A small minimum in the descending region gives way to a narrow maximum with a width smaller than 1 nm, and the specific features in the ascending region are weakly pronounced

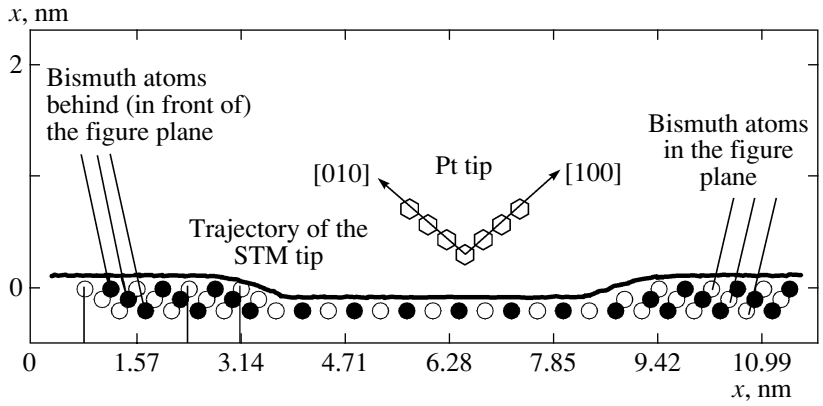

Fig. 5. Schematic diagram illustrating the arrangement of atoms in the cross section of the terrace boundaries. Open circles indicate atoms that are located in the figure plane and form atomic rows at the boundaries lying perpendicular to the figure plane. Closed circles represent atoms that lie off the figure plane and are shifted by one-half the atomic spacing along the normal to this plane. The solid line corresponds to the measured dependence $z(x)$. The tip for one of many possible orientations of the tip end at a distance characteristic of STM experiments is schematically shown above the surface. The scale along the x axis is represented so that the tick marks indicate the positions of bismuth atoms in the upper row. (The coincidence of numbers with a value of π is accidental!).

and only slightly exceed the noise level. (It should be noted that, since the initial current at a voltage of 0.64 V in these experiments is equal to 0.3 nA, the dependence $I(x)$ at close voltages tends to a constant level.)

The differences in the descending and ascending regions are quite natural because the bismuth structure determines the difference between the structures of the boundaries of the terraces facing each other, which should necessarily affect their physical properties (Fig. 5) [9]. It can be seen from Fig. 5 that the distance along the x coordinate between the nearest neighbor atoms lying in the figure plane, at the upper edge, and at the bottom on one side of the valley with a diatomic depth (for example, at the left) is equal to 2/3 of the atomic spacing along the scan line, whereas the corresponding distance on the other side of the valley amounts to 4/3 of the atomic spacing (i.e., the rows are shifted by 1 + 1.3 atomic spacings). In order to answer the question as to which of the above situations corresponds to the observed boundaries of the terraces, it is necessary that the atomic structure should be seen in the experiment. Unfortunately, atoms were not seen in the experiments under consideration. However, by comparing the experiments carried out at different times, we succeeded in revealing that the observed situation corresponds to that illustrated in Fig. 5, which will be discussed at the end of this section. If it is assumed that the bismuth–vacuum interface passes in the same way as is shown in this figure, i.e., through atoms lying in the figure plane (open circles), the actual trajectory of the STM tip in the situation illustrated in Fig. 5 corresponds fairly well to the predicted trajectory. It can be expected a priori that the transition regions should be considerably broadened, which is usually the case. Most likely, we were fortunate that the tip had a structure depicted in Fig. 5. For another possible orientation of the crystallite at the tip end, for example, in the [111] direction along the crystallite axis, the broadening is inevitable.

Let us return to the analysis of the tunneling spectra. Figure 6 shows the differential current–voltage characteristics averaged over the regions along the segments denoted by numerals in the upper topograms. This figure presents the results obtained for planar regions in which the tip shape must necessarily have no effect. Hence, the observed evolution of the differential current–voltage characteristics is undeniably associated with the change in the electronic spectrum of bismuth. At a distance of 6–8 nm from the midpoint of the steps, spectra *1* and *5* for both the descending (Fig. 6c) and ascending (Figs. 6d, 6e) regions almost coincide with spectrum *0* for regions far from the terrace boundaries. However, at a distance of 3–4 nm, the most characteristic peak at a voltage of +0.21 V (spectra *2*, *6*) is noticeably distorted. At a distance in the range 3.0–2.5 nm, the amplitude of this peak decreases significantly and the peak itself appears as the sum of two peaks at +0.21 and +0.19 V (spectra *3*, *7*). Finally, only the narrow pronounced peak at +0.19 V remains at the upper edge. The amplitude of this peak in the descending region (spectrum *4*) is somewhat larger than that in the ascending region (spectra *8*). It should be noted that the corresponding spectra measured for different steps (Figs. 6d, 6e) are nearly identical to each other.

A significant difference in spectra *4* and *8* is observed in the range close to zero voltage. More specifically, at zero voltage, the inflection in the differential current–voltage characteristic almost disappears in spectrum *4* and a well-defined peak with the maximum at –0.01 V appears in spectra *8*.

In the region of the boundaries themselves (Fig. 7), the spectra undergo substantial variations. Let us analyze some of these changes. In spectrum *9* (Fig. 7c), the amplitude of the peak at +0.19 V decreases significantly. Quite possibly, this peak is seen only because of

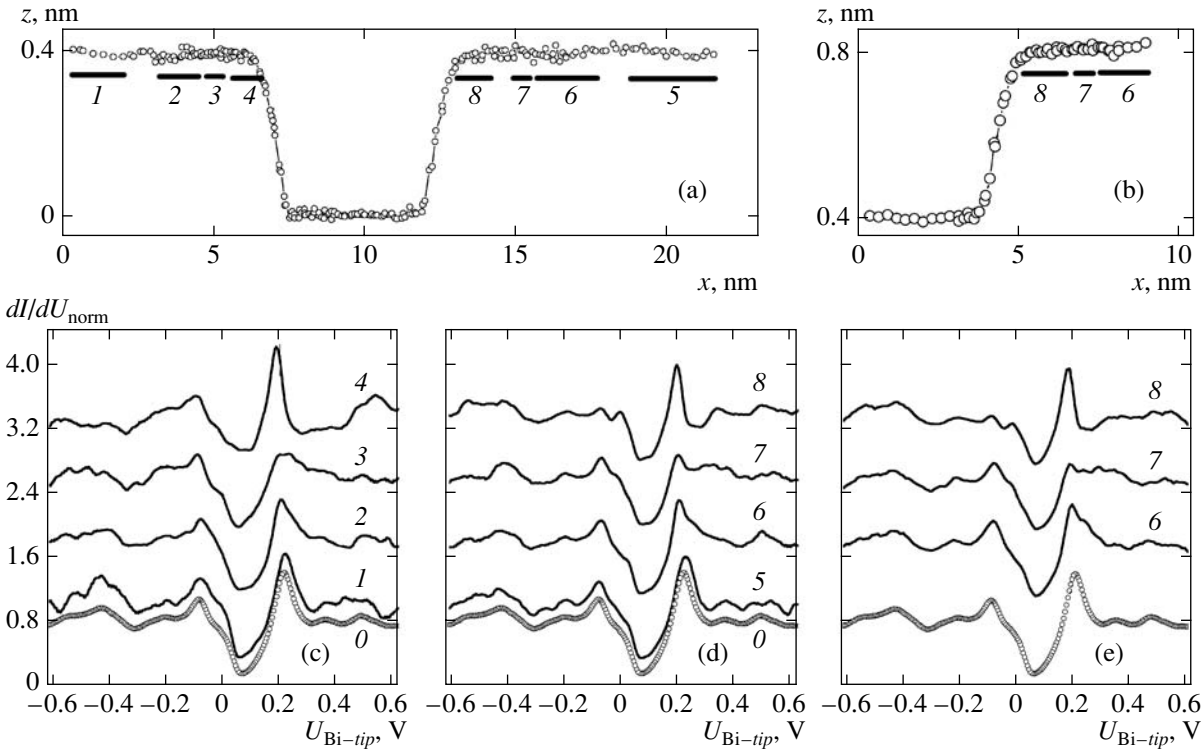

Fig. 6. Differential tunneling spectra averaged over the regions underscored by thick lines in panels (a) and (b). Numerals under these lines correspond to those in panels (c–e). The spectra indicated by the numeral *0* were obtained for planar regions far from the boundaries. The spectra shown in panels (c–e) are sequentially shifted along the *y* axis by 0.8, 1.6, and 2.4, respectively. The zeroth spectrum is shifted by –0.2.

the final resolution of the scanning tunneling microscope and corresponds to region *4*. However, there appears a peak at +0.08 V, which is observed only in this spectrum. In spectra *13* in Figs. 7d and 7e, the peak at +19 V remains almost identical to that in spectra *8*, but the peak at –0.08 V disappears, and the peak at –0.01 is shifted to +0.02 V. Spectra *12* in Figs. 7d and 7e, which seemingly correspond to the same regions, like spectra *11* in Figs. 7d and 7e, differ significantly. More specifically, spectrum *11* in Fig. 7e becomes similar to spectrum *0* for the planar surface. In spectrum *11* in Fig. 7d, the most characteristic peak at +0.21 V is split into two lines, a small peak arises at +0.07 V, and the inflection at zero voltage disappears. It is difficult to argue with confidence that spectra *12* are not a superposition of spectra *11* and *13*, even though the absence of the ascending portion characteristic of spectrum *13* at positive voltages suggests that this spectrum exhibits its own specific features. As regards spectrum *10* in Fig. 7c, the pronounced peak at +0.33 V and quite a different shape in the voltage range from –0.1 to +0.2 V indicate that the electronic system with a specific spectrum is formed at the lower edge of the valley.

It can be seen from the spectra measured at higher voltages (Fig. 8) that spectra *3* and *6* at the midpoints of the steps differ significantly both for the descending and ascending regions and from the spectra obtained for the planar regions (spectra *1* and *4* for the descending and ascending regions), where the spectra almost coincide with each other. It should be noted that, in spectrum *3*, the peaks at +1.6 and –0.5 V disappear and a peak at +0.6 V appears. A similar peak at +0.55 V is observed in spectrum *2* (this peak is also seen in spectrum *4* in Fig. 7). In spectrum *6*, maxima at +1.6 and +0.9 V give way to broader maxima at +1.50 and +0.75 V and the minimum at –0.7 V transforms into a maximum. It should also be noted that the spectra shown in Fig. 8 and those depicted in Figs. 6 and 7 can be compared taking into account that, in the voltage range from –0.4 to +0.4 V, the spectra are substantially broadened (by one order of magnitude) and distorted upon numerical differentiation, because we were interested in the behavior of the differential current–voltage characteristic at higher voltages. In order to increase the signal-to-noise ratio, it was necessary to perform the smoothing over the region with the width comparable to the width of the specific features at low voltages.

In conclusion of this section, we consider the spectrum obtained for the upper edge of the terrace in other series of measurements at higher initial currents (Fig. 9) in comparison with spectra *4* and *8* depicted in Fig. 6. The spectrum under consideration is of interest because it not only confirms the inference that the state different from the two-dimensional state observed far

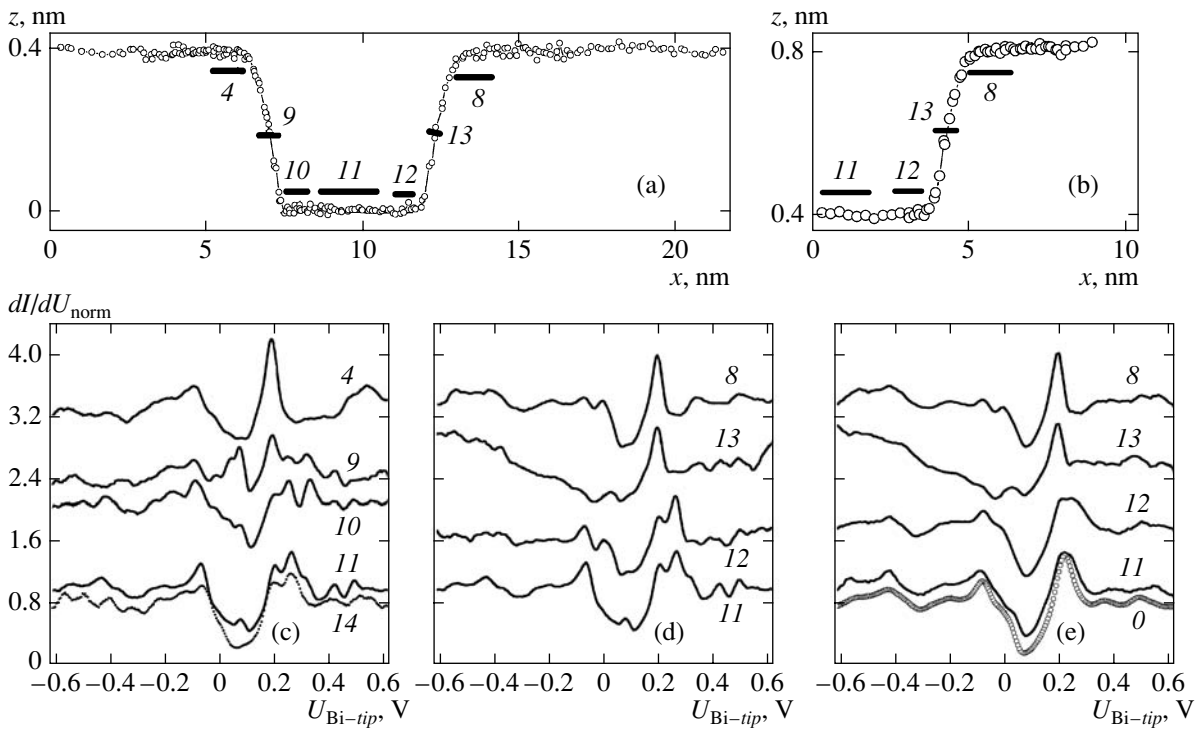

Fig. 7. Differential tunneling spectra averaged over the regions underscored by thick lines in panels (a) and (b). Numerals under these lines correspond to those in panels (c–e). The spectrum indicated by the numeral *0* was obtained for planar regions far from the boundaries. Spectrum *14* was recorded for the bottom of the valley at $x \approx 30$ nm (Fig. 3). The spectra shown in panels (c–e) are sequentially shifted along the *y* axis by 0.8, 1.6, and 2.4, respectively. The zeroth spectrum is shifted by –0.2.

from the boundary is formed at the boundary but also permits us to elucidate the crystallographic structure of the boundaries for the experiments from which the aforementioned results were obtained. As in spectrum *3* shown in Fig. 1, the peaks in spectrum *3* depicted in Fig. 9 are noticeably broadened as compared to those in spectra *4* and *8*. However, it is clearly seen that spectrum *3* at low voltages coincides with spectrum *8*: spectrum *3* contains the peak at a voltage close to zero, whereas spectrum *4* does not exhibit any features at these voltages. Therefore, spectra *3* and *8* correspond to the same crystallographic structure.

Unlike the experiments described above, in the experiments under consideration, we observed a well-defined atomic structure (Fig. 10), even though the measurements were performed with not a single-point tip and the resolution was considerably worse. In this case, the multipoint tip distorted the shape of the step in the descending region but does not affect the shape of the step upon changing over from the lower terrace (at the left of Fig. 10) to the upper terrace (at the right of Fig. 10), and the step height corresponded to the predicted value. It should be noted that the atomic structures in the lower and upper terraces are identical to each other. As can be seen from Fig. 10, the lower atomic rows are shifted with respect to the corresponding upper atomic rows by approximately 1/3 (0.31 ± 0.05) of the atomic spacing along the line of the shift in two halves of the image. Therefore, the atomic arrangement corresponds to that shown in Fig. 5.

4. DISCUSSION

The main qualitative conclusion which follows from the results obtained in this study lies in the fact that, at each boundary of atomic layers, there arises an electronic system with its own specific spectrum. This inference uniquely follows from the analysis of the tunneling spectra shown in Figs. 6–8. (The only exception is provided by spectrum *12* depicted in Fig. 7, which corresponds to the lower right boundary of the valley; however, this can be most likely associated with the shape of the scanning tip, which does not reach the required place.) For these states with characteristic energies (0.1–0.2 eV) reckoned from the Fermi level, the momenta along the straight boundaries should be relatively small (more specifically, they should be no larger than the transverse momenta). We can argue that, according to the evolution of the tunneling spectra (from spectrum *1* to spectrum *4* and from spectrum *5* to spectrum *8*) (Fig. 6), the momentum of electrons from the valence band with a maximum in the vicinity of 0.2 V should be approximately equal in order of magnitude to $(\pi/2) \times 10^{-7}$ cm^{-1}. Hence, electrons along the boundaries are delocalized over distances larger than the interatomic distance and, in this sense, we can speak

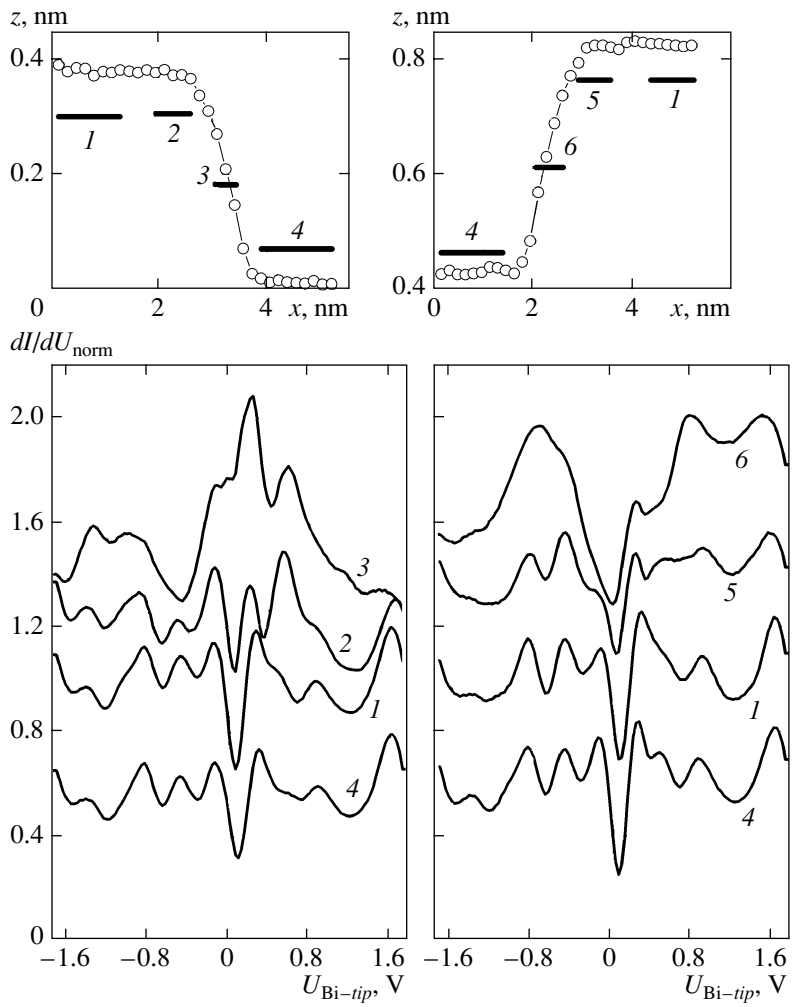

Fig. 8. Differential tunneling spectra averaged over the regions underscored by thick lines in the upper panels. Numerals under these lines correspond to the spectrum numbers in the lower panels. In the lower panels, the zero level for spectra *1* corresponds to zero in the *y* axis; spectra *2*, *5* and *3*, *6* are shifted along this axis by 0.4 and 0.8, respectively; and spectra *4* are shifted downward by –0.4.

about one-dimensional systems. An additional argument is that the STM tip moves in the course of scanning at an angle different from the right angle with respect to the boundary and the spectra are recorded at different points of atomic chains. Moreover, there is a small drift (of the order of the interatomic distance) in sequential measurements of the set of spectra. Therefore, the coincidence of the spectra for different steps counts in favor of the electron delocalization.

However, a number of questions remain open. In particular, the maximum observed at a voltage of –0.08 V in the differential current–voltage characteristic is present in all tunneling spectra and does not undergo substantial changes. According to its position, this maximum is in satisfactory agreement with the position of the bottom of the electronic band for two-dimensional electrons. However, the insensitivity to the height difference most likely indicates that the wave function of this state extends from the surface deep into the bulk of the material.

Spectra *9* and *13* in Fig. 7 are inconsistent with the simple interpretation based on the uncertainty principle. The peak at a voltage of +0.08 V, which is characteristic of spectrum *9*, is absent in spectra *4* and *10* for the neighboring regions located at a distance of the order of 1 nm. If this value is substituted into the formula for the transverse momentum, the energy (for the free-electron mass) is estimated to be 0.5 V. The specific feature observed at voltages of 0.01–0.02 V in spectrum *13* agrees even worse with the above scheme. Quite possibly, the point is that, according to the schematic diagram depicted in Fig. 5, different atoms of the tip end (and, hence, states with different symmetries) participate in the formation of the tunneling current during recording of differential current–voltage characteristics *9* and *4, 10*.

Spectrum *11* in Fig. 7 requires special consideration. This spectrum was measured for the planar region at the center of the valley; however, it differs significantly from the spectrum measured for the planar regions far

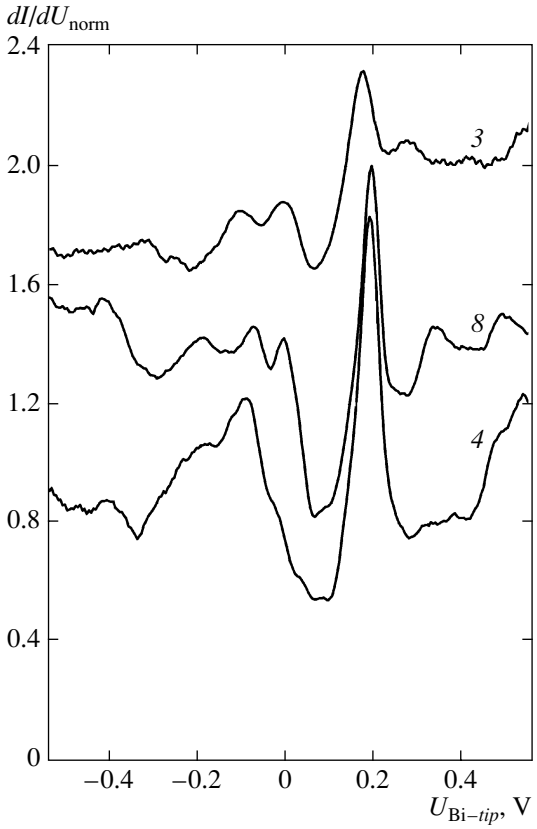

Fig. 9. Differential tunneling spectra for the tip position at the upper terrace edge. Spectrum *3* was obtained under the same conditions as spectrum *3* of the planar region presented in Fig. 1. Spectra *4* and *8* are identical to those shown in Fig. 6. The zero level for spectrum *4* corresponds to zero in the *y* axis. Spectra *8* and *3* are shifted along this axis by 0.4 and 0.8, respectively.

from the terrace boundaries (spectrum *0* in Fig. 6). Moreover, the fact stands out that the most characteristic peak in the vicinity of +0.2 V is split into two peaks. This specific feature could be associated with the quantum confinement due to the closeness of the boundaries on both sides. The momentum of the relevant electrons was estimated above. Knowing their energy, we can estimate the effective mass as 0.3 of the free-electron mass. If instead of the size of 2 nm, we use the valley width of approximately 5 nm (Fig. 7) in the above estimation, the characteristic energy of quantum confinement appears to be $0.2(2/5)^2$ meV $\approx$ 30 meV. With allowance made for the crudeness of the obtained estimate, this value differs insignificantly from the observed splitting of the peak at a voltage $U \approx +0.2$ V. However, spectrum *14* in Fig. 7 for the bottom of the narrower valley at $x \approx 30$ nm (Fig. 3) closely resembles spectrum *11*, even though the width of this valley is two times smaller than that obtained at $x \approx 60$–70 nm.

In our case, the investigation of linear one-dimensional structures should necessarily include an analysis of the mechanisms of transitions of electrons from one-dimensional states to two-dimensional states and then to three-dimensional states. In order to evaluate the role of these processes, as well as to calculate the tunneling current, we should calculate the energy spectrum of the aforementioned states (and to consider models of the spectrum of the tip), which is far beyond the scope of our present paper. However, we can assume that the processes of current spreading are not very significant because the spectra obtained at different currents (Figs. 1, 9), i.e., upon a considerable change in the resistance of the tunneling gap (one of the obstacles to the current flow), are similar to each other.

ACKNOWLEDGMENTS

The author would like to thank A.F. Andreev for his interest expressed in this study, A.V. Ofitserov for his participation in performing the measurements, and V.I. Marchenko for his participation in discussions of the results obtained in this work and for a number of helpful remarks.

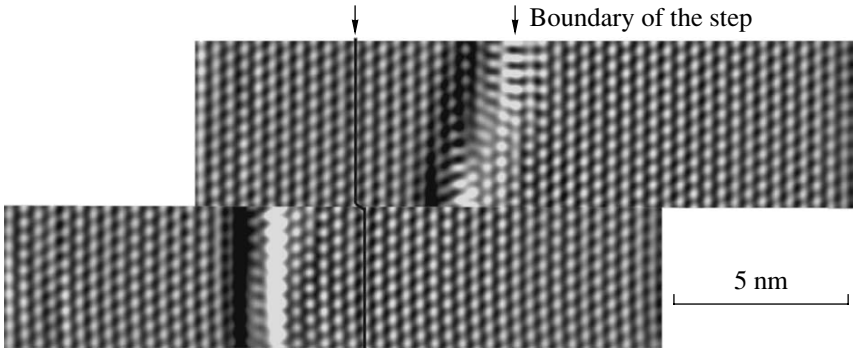

Fig. 10. Differentiated and smoothed (using the two-dimensional Fourier filtration) STM image of the surface in the region of the terrace boundary. Spectrum *3* was obtained for the tip position at the upper terrace (the region to the right of the boundary) at a distance of the order of 1 nm from the midpoint of the step. For a clear illustration of the displacement of the atomic rows of the lower terrace (the region at the left) with respect to the upper terrace, the image was cut along the line passing through the middle of bright dots ("atoms") and the lower part is shifted with respect to the upper part so that the atomic rows at the right are brought into coincidence. The broken line indicated by the arrow passes through the nearest rows containing "cut atoms." It can be seen that the relative displacement of the rows is approximately equal to 1/3 of the atomic spacing along the displacement line.

This study was supported by the Russian Foundation for Basic Research (project nos. 04-02-17369-a and 07-02-00515-a).

REFERENCES

1. V. S. Édel'man, Usp. Fiz. Nauk **123**, 257 (1977) [Sov. Phys.—Usp. **20**, 819 (1977)].
2. Y. Lin and R. E. Allen, Phys. Rev. B: Condens. Matter **52**, 1566 (1995).
3. A. V. Ofitserov and V. S. Edel'man, Zh. Éksp. Teor. Fiz. **120** (3), 731 (2001) [JETP **93** (3), 642 (2001)].
4. G. Jezequel, J. Thomas, and I. Pollini, Phys. Rev. B: Condens. Matter **56**, 6620 (1997).
5. Ch. R. Ast and H. Höchst, Phys. Rev. B: Condens. Matter **67**, 113102 (2003).
6. Yu. M. Koroteev, G. Bihlmayer, J. E. Gayon, et al., Phys. Rev. Lett. **93**, 046403 (2004).
7. T. K. Kim, J. Wells, C. Kirkegaard, et al., Phys. Rev. B: Condens. Matter **72**, 085440 (2005).
8. A. M. Troyanovskiĭ and V. S. Édel'man, Zh. Éksp. Teor. Fiz. **115** (6), 2214 (1999) [JETP **88** (6), 1212 (1999)].
9. A. M. Troyanovskii and V. S. Edel'man, Kristallografiya **44** (2), 336 (1999) [Crystallogr. Rep. **44** (2), 300 (1999)].
10. V. S. Edelman, D. Yu. Sharvin, I. N. Khlyustikov, and A. M. Troyanovskii, Europhys. Lett. **34**, 115 (1996).
11. V. S. Edel'man, Usp. Fiz. Nauk **175** (10), 1111 (2005) [Phys.—Usp. **48** (10), 1057 (2005)].
12. M. S. Khaĭkin, S. M. Cheremisin, and V. S. Édel'man, Prib. Tekh. Éksp., No. 4, 225 (1970) [Instrum. Exp. Tech., No. 4, 1222 (1970)].
13. I. N. Khlyustikov and V. S. Edel'man, Prib. Tekh. Éksp., No. 1, 158 (1996) [Instrum. Exp. Tech. **39** (1), 143 (1996)].
14. V. S. Edel'man, A. M. Troyanovskii, M. S. Khaikin, et al., J. Vac. Sci. Technol., B: Microelectron. Nanometer Struct.—Process., Meas., Phenom. **9**, Part 2, 618 (1991).
15. A. V. Ofitserov and V. S. Edel'man, Prib. Tekh. Éksp., No. 2, 133 (2005) [Instrum. Exp. Tech. **48** (2), 259 (2005)].
16. J. A. Stroscio and R. M. Feenstra, in *Scanning Tunneling Microscopy*, Ed. by J. A. Stroscio and W. J. Kaiser (Academic, San Diego, CA, United States, 1993), p. 95.

Translated by O. Borovik-Romanova